

SROC: Space Rider Observer Cube Mission

Original

SROC: Space Rider Observer Cube Mission / Deva, Luca; Ammirante, Giorgio; Taiano, Giorgio; Bassissi, Enrico; Parigi, Federico; Corpino, Sabrina; Stesina, Fabrizio; Niero, Luca; Lovaglio, Lucrezia; Rotti, Valentina; Branz, Francesco; Sansone, Francesco; Topputo, Francesco; Panicucci, Paolo; Lunghi, Paolo; Pirat, Camille; Van Den Eynde, Jeroen; Vergallo, Giulia. - ELETTRONICO. - (In corso di stampa). (Small Satellites Systems and Services Symposium 2026 Pula (Ita) 4-8 May 2026).

Availability:

This version is available at: 11583/3010728 since: 2026-05-12T09:04:07Z

Publisher:

SPIE

Published

DOI:

Terms of use:

This article is made available under terms and conditions as specified in the corresponding bibliographic description in the repository

Publisher copyright

SPIE postprint/Author's Accepted Manuscript e/o postprint versione editoriale/Version of Record con

(Article begins on next page)



Proximo-distal medial gastrocnemius neuromechanical behavior: combining HDsEMG with SSI elastography

Marco Daghero^{a,d,*}, Maria Clara Albuquerque Brandão^b, Mara Terzini^{a,d},
Taian Martins Vieira^{c,d}, Liliam Fernandes de Oliveira^b

^a Department of Mechanical and Aerospace Engineering, Politecnico di Torino, Turin 10129, Italy

^b Biomedical Engineering Program, Federal University of Rio de Janeiro, Rio de Janeiro 21941-914, Brazil

^c LISiN-Department of Electronics and Telecommunications, Politecnico di Torino, Turin 10129, Italy

^d Polito^{BIO}Med Lab, Politecnico di Torino, Turin 10129, Italy

ARTICLE INFO

Keywords:

Electromyography
Muscle excitation
Muscle shear modulus
Muscle stiffness
Shear wave elastography

ABSTRACT

The medial gastrocnemius (MG) plays a crucial role in lower limb biomechanics, yet its pennate architecture and regional variations in excitation complicate its neuromechanical characterization. This study investigates whether the relationship between muscle excitation and stiffness is region-specific within MG, by combining high-density electromyography (EMG) and SuperSonic Imaging (SSI) elastography. Eighteen participants performed low-level, force-increasing contractions while EMG amplitude and shear modulus (μ) were concurrently measured in proximal and distal regions of the MG. The distribution of channels detecting EMGs with greatest amplitude values revealed regional differences in MG excitation, with more distal fibers being recruited as force requirement increased. A strong correlation was found between EMG envelope amplitude and μ across all subjects for both portions (mean \pm std: $r = 0.85 \pm 0.06$ proximally; $r = 0.91 \pm 0.05$ distally). Moreover, Fisher-transformed correlation coefficients were significantly lower ($p = 0.004$) in the proximal portion (mean \pm std: $r_f = 1.32 \pm 0.26$) compared to the distal one ($r_f = 1.63 \pm 0.34$). This difference indicates that the preferential recruitment of distal fibers during increasing contraction drives a more consistent relationship between excitation and stiffness in the distal MG relative to the proximal region. These findings underscore the importance of considering muscle region-specificity when assessing MG excitation and stiffness, and highlight the value of combining high-density EMG and SSI for a comprehensive neuromechanical assessment of muscle function.

1. Introduction

The medial and the lateral gastrocnemius, along with the soleus muscle and the Achilles tendon, form the triceps surae complex. This complex produces torque in the sagittal and frontal planes [1] and is involved in many daily activities, from the maintenance of the standing posture [2] to running [3]. Within this complex, the medial gastrocnemius (MG) presents distinct anatomical and functional characteristics with respect to lateral gastrocnemius and soleus. The soleus is typically described as a tonic muscle, specialized for endurance and postural control, whereas the MG has a greater capacity for rapid force generation, making it essential for both postural and dynamic tasks [4]. Although the lateral gastrocnemius is structurally similar to the MG, its functional contribution is less pronounced: Héroux et al. [5] showed that

selective lateral gastrocnemius fatigue has negligible effects on balance, indicating a minor role in postural control compared to MG and soleus. Additionally, the MG is larger in volume and displays greater architectural heterogeneity than the lateral gastrocnemius, with fascicle orientation and excitation patterns varying along its proximo-distal axis [6,7]. Due to its singular architecture and significant role in lower limb biomechanics, accounts on the MG excitation [8,9] and mechanical properties [10,11] are commonplace in the literature. In particular, its pronounced heterogeneity makes the MG especially suitable for concurrent examination of regional variations in neuromuscular excitation and mechanical properties. Such an investigation requires methods sensitive to spatial changes in both domains.

High-density surface electromyography and SuperSonic Imaging (SSI) dynamic elastography are two techniques likely suitable for such

* Corresponding author at: Department of Mechanical and Aerospace Engineering, Politecnico di Torino, Turin 10129, Italy.

E-mail addresses: marco.daghero@polito.it (M. Daghero), mclara@peb.ufrj.br (M.C. Albuquerque Brandão), mara.terzini@polito.it (M. Terzini), taian.martins@polito.it (T.M. Vieira), liliam@peb.ufrj.br (L.F. de Oliveira).

<https://doi.org/10.1016/j.bspc.2026.110450>

Received 28 March 2025; Received in revised form 23 January 2026; Accepted 21 April 2026

Available online 28 April 2026

1746-8094/© 2026 The Author(s). Published by Elsevier Ltd. This is an open access article under the CC BY license (<http://creativecommons.org/licenses/by/4.0/>).

purpose. The former technique consists of sampling high-density electromyograms (EMGs) with an array of electrodes placed over the skin surface [12]. The multiple-electrode configuration allows sampling from a large volume of the target muscle, mapping the distribution of the electric potential on the skin and thus enabling a more detailed analysis of regional patterns of muscle excitation [13,14]. On the other hand, SSI enables the assessment of muscle mechanical properties by computing the muscle shear modulus (μ), which is proportional to tissue stiffness. This is achieved in real time, by indexing colors within a region of interest superimposed on the B-mode ultrasound image. SSI operates in two primary modes. The pushing mode utilizes high-intensity acoustic radiation forces directed at various tissue depths, inducing shear waves within the tissue [15]. Simultaneously, the imaging mode captures the propagation speed of these shear waves (c_s). Under the assumption of tissue isotropy and pure elasticity, μ can be computed directly as $\mu = \rho c_s^2$ (1), with $\rho = 1010 \text{ kg/m}^3$ being the density of the biological tissue [16,17].

The putative view that excitation leads to stiffening of the muscle tissue has been documented by combining SSI with the traditional, single-pair-of-electrodes EMG approach. In particular, muscle shear modulus has been shown to scale with bipolar EMG amplitude in fusiform muscles [18–20]. However, collecting similar evidence for the in-depth pennate MG muscle [14] is not straightforward. First because EMGs detected from a single skin location in bipolar derivation reflect the excitation of fibers residing nearby the detection electrodes [21]. Any attempt to relate μ to EMG amplitude would thus need to be limited to the muscle region sampled concurrently by both EMG electrodes and the SSI probe. Second, no fixed proximo-distal pattern of excitation has been established for MG. This variability may arise from regional differences in muscle architecture, motor unit distribution, and task-dependent neural strategies, which can differentially modulate activation along the muscle length [8]. It seems though that the muscle distal fibers are predominantly excited during small intensity contractions (e.g. standing, [9]), while the opposite was reported during low-level stimulation of the tibial posterior nerve [7,9].

Previous SSI-EMG studies [22] have implicitly assumed that muscle excitation is spatially homogeneous, justifying the assessment of EMG and shear modulus in a single region. Yet, electrophysiological and ultrasonographic evidence indicates that this assumption does not hold for the MG, which exhibits heterogeneous excitation [7] and architecture [6] along its length. If local SSI-EMG relationships differ across regions, then results from a single site may not represent the whole muscle. It seems therefore that only through the concurrent use of SSI and HDsEMG would it be possible to unambiguously assess local relationships between GM μ and excitation.

To address this gap, from high-density EMGs and SSI data we investigate whether changes in MG stiffness are associated with changes in excitation, in spite of any proximo-distal variations in MG excitation. We hypothesized that (i) EMG amplitude would increase differently along the proximo-distal axis during a low-level force-increasing isometric contraction, and (ii) this regional difference in excitation would lead to region-specific EMG-shear modulus relationships. Indeed, if excitation increased similarly in proximal and distal regions, the EMG- μ relationship would be comparable between regions; conversely, region-specific excitation patterns are expected to result in different EMG- μ relationships along the muscle length. In addition to strengthen the value of a combined SSI-EMG approach to characterize the muscle neuromechanical properties, our results may be of great applied value. Confirmation of our hypothesis likely implies that with: i) high-density EMG, changes in excitation of superficial muscles may be assessed proximo-distally and medio-laterally; ii) SSI, changes in shear modulus associated with changes in excitation may be assessed in proximo-distal and deep-superficial directions; iii) a combined approach, changes in excitation may be assessed concurrently both within and between muscles.

2. Methods

2.1. Participants

A total of 18 subjects (7 women and 11 men; 25 ± 4 years; 74 ± 17 kg; 173 ± 9 cm), reporting no history of major lower limb injuries, participated in this study after providing written informed consent. Experimental procedures conformed to the standards set by the Declaration of Helsinki and were approved by the Ethics Committee of the Clementino Fraga Filho University Hospital (HUCFF/UFRJ, n°: 7.223.170).

2.2. Experimental protocol

After being instructed about the experimental procedures, participants were asked to sit comfortably on an isokinetic dynamometer (Biodex 4 System Pro Medical System Inc, New York, USA) with the right knee fully extended and the hips flexed at 85° (Fig. 1A). The right lateral malleolus was aligned coaxially with the dynamometer's axis of rotation and the foot was secured with Velcro straps to the support platform with the ankle at 5° of plantar flexion (Fig. 1A).

Initially, the participants performed two maximal voluntary isometric contractions (MVIC), lasting 5 s each and with 2-min rest in between. The maximum peak torque between the two MVICs was used to scale the contraction level for the subsequent tasks: an isometric contraction of linearly increasing intensity from 0 to 30% MVIC for 60 s. The ramp contraction was limited to 30% MVIC to minimize fatigue and ensure stable recording conditions compatible with the temporal resolution of SSI elastography (~ 1 Hz). To perform this task, the participants received real-time visual feedback of the generated force via a monitor placed 3 m away from them. The same task was repeated four times, with the elastography transducer placed two times in the proximal portion and two times in the distal portion (random order, breaks of 2 min, Fig. 1A; cf. below for the definition of proximal and distal portions). Before the start of the experimental protocol, familiarization trials were conducted until, based on visual inspection, the participant was able to modulate the ankle torque according to the required ramp profile.

2.3. High-density EMG and SSI measurements

Ultrasound imaging (Aixplorer v.11, Supersonic Image, Aix-en-Provence, France) with a 40 mm linear transducer at 2–10 MHz frequency was used to identify the boundaries of the MG muscle and thus standardize EMG electrodes and SSI probe positioning. For each subject, the right leg length (l_{leg}) was measured as the distance between the popliteal crease and the lateral malleolus [23]. Initially, the ultrasound transducer was positioned transversely at $0.3l_{leg}$ to identify the medial and lateral MG boundaries. Then, a longitudinal, reference line was drawn midway between the MG medio-lateral boundaries. With the transducer positioned along the reference line, the proximal insertion was identified by sliding the transducer in the proximal direction.

High-density EMGs were collected using a linear electrode array with 32 electrodes (5 mm inter-electrode distance: IED). A conductive paste (AC Cream, Spes Medica, Genoa, Italy) was spread over the cavities of the adhesive pad securing the grid of electrodes to the skin, after shaving and cleaning the skin with abrasive paste (Nuprep – Skin Prep Gel, Weaver and Company, Colorado, USA). The array was aligned parallel to the MG longitudinal axis, with the most proximal electrode placed 2 cm distal to the proximal insertion and 2 cm medial from the reference line: with this positioning procedure we could center the SSI transducer on the MG midline.

HDsEMG and SSI were conducted simultaneously on the MG to ensure a direct, synchronized assessment of muscle excitation and stiffness. Monopolar EMGs were sampled at 2000 Hz, with a fixed 1 V/V gain. EMGs and the force signal provided by the dynamometer were

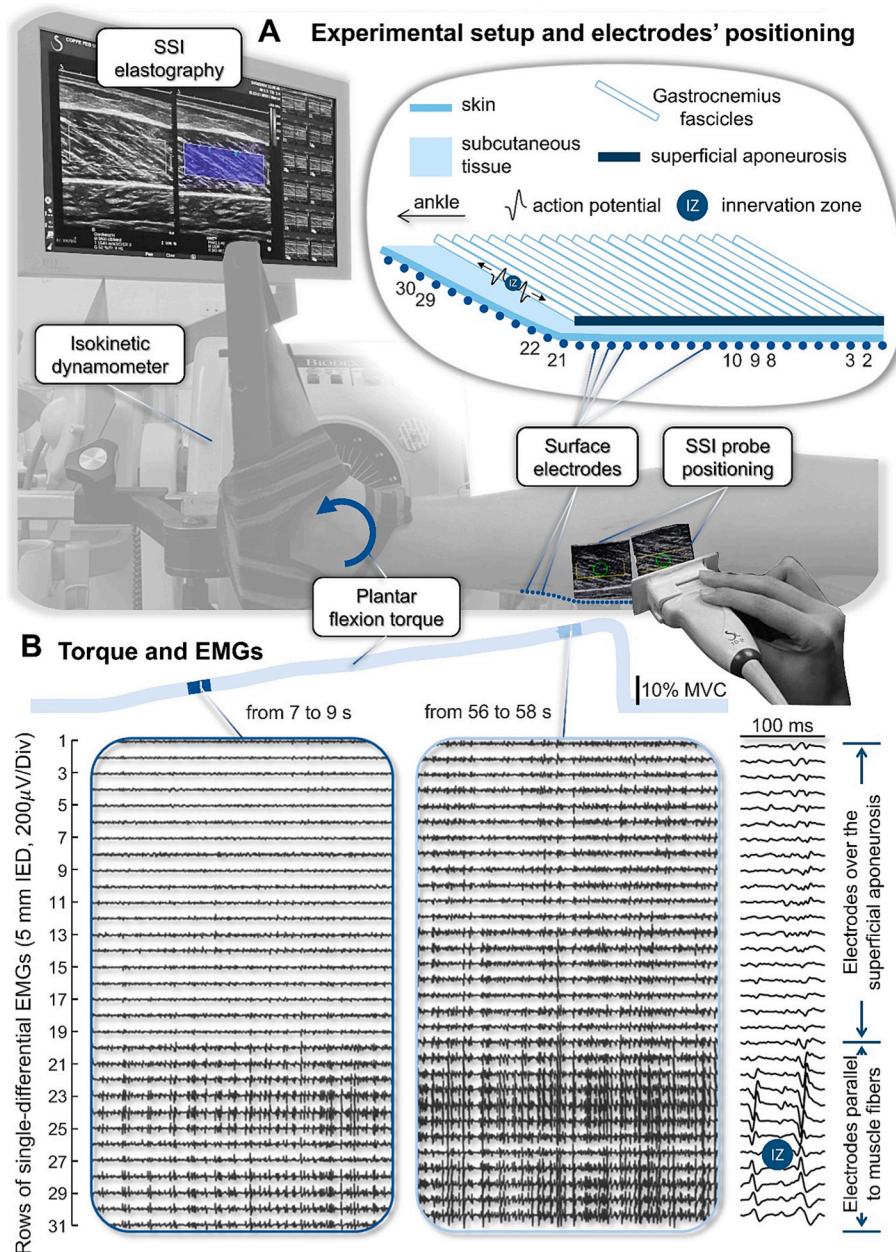


Fig. 1. (A) Experimental setup for voluntary isometric contraction and positioning of the transducers used for simultaneous acquisition of EMG and SSI elastography from the MG muscle. (B) Torque and single-differential EMGs for one subject during 60 s of isometric contraction, from 0 to 30% MVIC. Innervation zone (IZ) and action potential propagation can be appreciated in the 100 ms expanded view (right column).

digitized concurrently using a 24-bit A/D converter (MuoviPro, OT Bioelettronica SRL, Turin, Italy). For the SSI acquisition, the preset used was MSK-adapted, with an opacity of 100%, 90% gain, SWE opt. setting in penetration mode, persistence off and the SWE box with dimensions of 1.0×3.3 cm, which included a μ scale ranging from 0 kPa to the transducer fullscale, 100 kPa: from 0 to 300 kPa in terms of Young's modulus. The SWE box was positioned entirely within the muscle tissue, carefully avoiding the superficial aponeurosis, and the maximum depth was limited to 3 cm. Acoustic coupling gel (Ultrex gel; Farmativa Industria e Comercio Ltda, Rio de Janeiro, Brazil) was applied to the skin surface to ensure proper contact, with a custom-made 3D-printed accessory to maintain a consistent gel thickness of 3 mm between the transducer and the skin. The elastography video started 5 s before the beginning of the submaximal contractions, concurrently with the EMG data acquisition. However, the Aixplorer equipment has a video recording limit of 60 s. Therefore, elastography data were acquired up to

27.5% of the MVIC (55 s), and data analysis was restricted to this interval.

2.4. Assessing spatial inhomogeneities in MG excitation

To assess spatial variations in MG excitation, the EMG processing pipeline followed three main steps: (i) preprocessing of monopolar signals, (ii) calculation of subject-specific bipolar EMGs, and (iii) quantification of regional excitation via channel segmentation and centroid estimation.

- 1. Preprocessing of monopolar EMGs.** Monopolar signals were band-pass filtered (15–350 Hz, 8th-order Butterworth) to remove motion artifacts and high-frequency noise while preserving the physiological frequency content [9,24]. Then, single-differential signals (Fig. 1B) were calculated by subtracting consecutive rows of electrodes (5 mm

IED). From these differential signals, electrodes positioned over the superficial aponeurosis were identified and retained for further analysis, whereas electrodes over the propagation zone (Fig. 1B) were discarded [9,25].

2. **Calculation of subject-specific bipolar EMGs.** Bipolar EMGs were computed using a subject-specific IED to maximize sensitivity to the target muscle fibers while minimizing contamination from adjacent muscles, as we recently demonstrated [26]. Based on the view that bipolar electrodes sample action potentials within 1 IED from the center of the pair of electrodes [26,27], we computed bipolar EMGs considering the minimal possible IED greater than the subcutaneous thickness measured separately for the proximal and distal regions according to [28] (cf. d_p and d_d in Fig. 2C). Specifically, the criteria

$IED > d_p$ and $IED > d_d$ were applied. Distributions of subcutaneous thickness and resulting electrode distances are reported in the Supplementary Material (Table S1). This procedure provided a variable number of consecutive channels, computed from the monopolar signals. The EMG envelope was obtained by full-wave rectifying and low-pass filtering each bipolar EMG (2 Hz cutoff, 6th-order Butterworth) to emphasize slow-varying changes in excitation, consistent with the 0.5% MVIC/s ramp protocol.

3. **Quantification of regional excitation.** Each 60-second ramp contraction was divided into three consecutive 20-second intervals, representing submaximal contractions at 0–10%, 10–20%, and 20–30% MVIC. Within each interval, the EMG envelopes were averaged over time, and channels were segmented if their mean

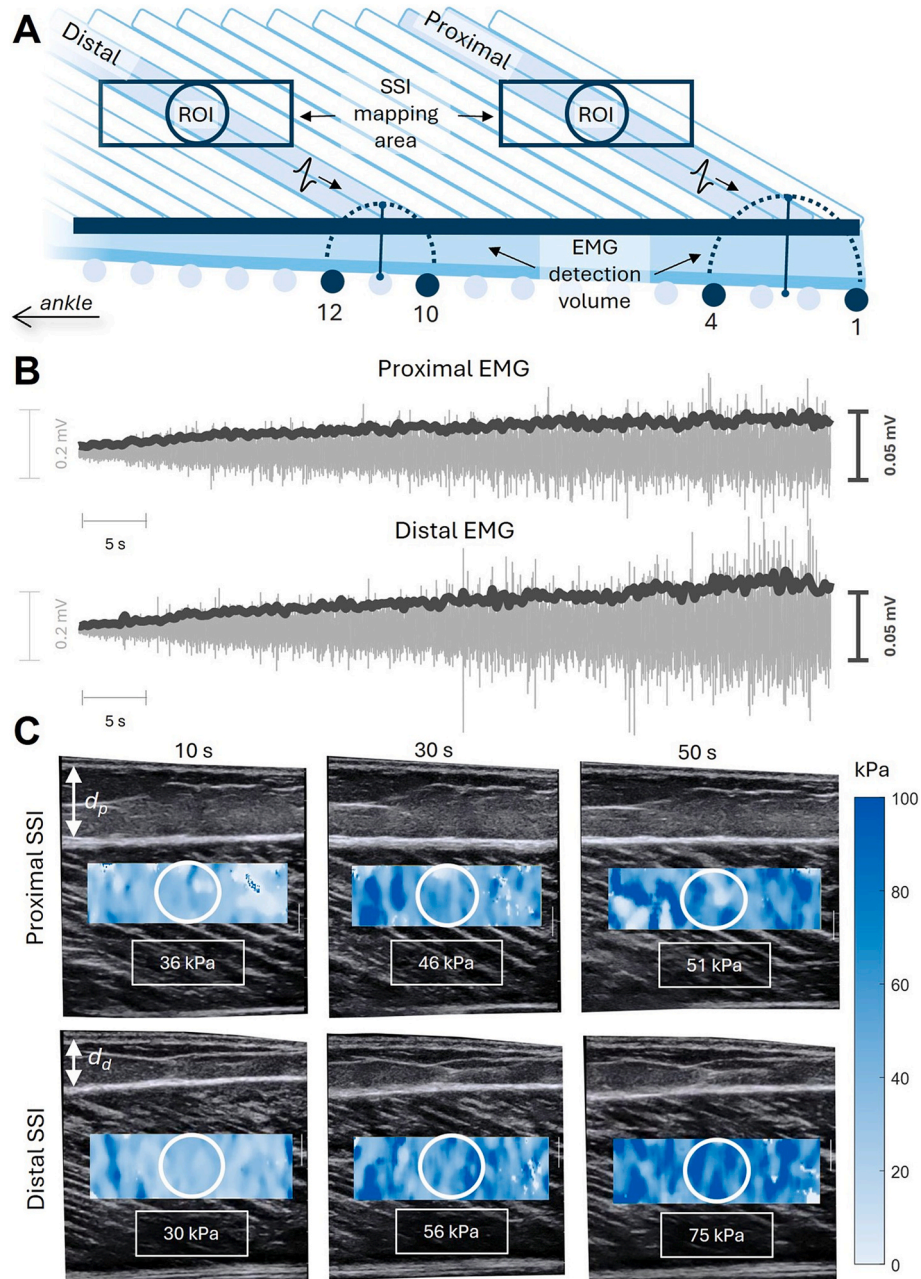


Fig. 2. (A) Identification of proximal and distal regions for SSI and EMG comparison. Semicircles were plotted based on the direct relationship between the surface potential amplitude and the IED radial distance from the center of the electrode pairs. (B) Bipolar EMGs (light gray) from proximal and distal portions of MG muscle, with the corresponding envelopes overlaid (dark gray), recorded for a single subject. (C) Frames from elastography videos at 10 s (5% MVIC), 30 s (15% MVIC) and 50 s (25% MVIC) are shown, displaying shear wave elastography color maps and the resulting average μ within the ROI. Subcutaneous thickness for the proximal (d_p) and distal (d_d) regions used for defining IED.

amplitude exceeded 70% of the maximum amplitude across all channels in the proximal and distal regions [29]. The centroid of the resultant distribution of excitation was then calculated as the weighted average of the coordinates of the segmented channels. To contend with inter-individual variability, the centroid coordinates were normalized to the muscle length, from the proximal insertion to the most distal electrode over the superficial aponeurosis.

2.5. Evaluating the relationship between MG excitation and shear modulus

Shear moduli were computed from elastography videos exported in AVI format with the ElastoGUI open software (<https://bio.tools/elastogui>). A circular region of interest (ROI) with a diameter of 1 cm was placed at the center of the mapping area and considered for the processing of all frames (Fig. 2A), to ensure methodological standardization and precise spatial correspondence between mechanical and neural measurements. Each indexed color inside the mapping area represents a value of measured c_s which was converted to μ based on equation (1). The average μ inside the ROI was then computed for each frame of the elastography videos. The elastography videos were processed in real time at approximately 1 Hz (min: 0.8 Hz, max: 1.2 Hz). The ElastoGUI software provides information on the number of processed frames in each video and the percentage of unfilled (% void) and saturated (% saturation) pixels within the ROI. Void pixels can result from low signal-to-noise ratio and poor shear wave generation, typically due to high attenuation and shadowing, motion artifacts or depth and angle issues [30,31]. Conversely, saturation occurs when shear wave speed exceeds the probe's range, due to localized tissue stiffness. Since all of these artifacts affect the system's ability to accurately detect and process shear wave propagation, some frames were excluded from the analysis based on these two parameters (% void > 2% and % saturation > 2%; similar to [32,33]) and based on visual inspection of elastography videos. Visual inspection consisted of assessing B-mode image quality and identifying eventual motion artifacts by an experienced operator. Importantly, visual inspection was performed blindly, before any extraction or visualization of shear modulus (μ) values or HDsEMG data. During this phase, the operator had access only to the elastography video, thus eliminating potential bias related to knowledge of contraction dynamics or outcome measures. This approach ensured that the selected trials reflected valid mechanical properties, unaffected by signal dropout due to the equipment's processing limitations. After this step, for each pair of ramps (corresponding to proximal or distal position of the elastography transducer), the ramp with the highest number of remaining frames, indicating a higher quality of recording, was considered for further analysis. The routine as well provides the exact time points in the elastography video when the μ values were analyzed, which were used to synchronize the data with HDsEMG.

For comparing the EMG envelope with the temporal changes in μ for the proximal and distal regions separately, only the bipolar EMGs obtained from the two electrode pairs centered at the ending of muscle fibers where μ was computed were considered for analysis, using the minimal possible IED greater than d_p and d_d , respectively. These electrodes were identified manually by visually tracking the fascicles within the μ processing region up to the superficial aponeurosis in ultrasound images, as illustrated in Fig. 2A (e.g., electrodes 1 and 4 for the proximal region, and electrodes 10 and 12 for the distal region). The use of a single, centrally located ROI was motivated by the need to preserve spatial correspondence between elastography and EMG measurements, as positioning multiple ROIs along the muscle could have resulted in ROIs without corresponding underlying electrode pairs. After this process, two EMG envelope curves (proximal and distal) were obtained (Fig. 2B) and evaluated at the time instants corresponding to the elastography measurements (Fig. 2C).

2.6. Statistical analysis

The distributions of the normalized centroid and the % of segmented channels were tested for normality using the Shapiro-Wilk test, which indicated a non-Gaussian distribution ($p = 0.002$). Thus, non-parametric statistic (Friedman test) was used to test the effect of the increasing force on these two variables, during the three contraction intervals. To determine the direction of this effect, the Wilcoxon Signed-Rank Test, with Bonferroni-Holm correction, was considered for the pairwise comparison between the three intervals. On the other side, after ensuring the distributions of EMG envelope and μ values were Gaussian (Shapiro-Wilk test, $p > 0.212$), Pearson correlation coefficient between both variables was computed: based on previous studies [18,34,35], we expect a linear relationship between EMG amplitude and the shear modulus. The Pearson correlation coefficient, after Fisher transformation (r_f), and the maximum thickness of the adipose tissue above the muscle (d_p and d_d) were then compared between proximal and distal portions using the paired t -test. The significance level was set at $p < 0.05$.

3. Results

3.1. Heterogeneous MG excitation

Regarding the distribution of excitation along MG, Table 1 presents the normalized centroid and the % of segmented channels for all 18 subjects. The centroid was on average located at the distal half of the muscle tissue sampled. Friedman test revealed a significant effect of force level on the centroid metric ($p = 0.002$), indicating that different muscle regions were excited as force requirements increased. The centroid displacement between interval 1 and interval 3 ($p = 0.012$) reflects the greater increase in the EMG envelope observed in the distal portion (cf. Fig. 3A-B). Finally, the % of segmented channels varied considerably across subjects (interquartile range > 33%), with the median remaining well below 100% (Table 1).

3.2. The EMG amplitude and shear modulus relationship is region-specific

Fig. 2B-C presents raw data from a representative subject. During the 60 s of isometric contraction, EMG amplitude increased in both proximal and distal MG portions, with a notably greater increase in the distal portion. Similarly, the μ values increased from contraction start to end, as evidenced by the comparison of the colormaps at 10 s (5% MVIC), 30 s (15% MVIC) and 50 s (25% MVIC). The temporal trends of EMG envelope and μ are more clearly illustrated in Figs. 3A-D, for the same representative subject. The dependence of EMG amplitude and μ values on time—and thus on contraction intensity—is more clearly evident in Fig. 3A-D. Even though the temporal increase in EMG envelope and μ values is clear for the two regions, envelope and μ values obtained distally at the end of the contraction were nearly twice as high as those obtained proximally (cf. data points at about 50 s in Fig. 3A-D). This region-specific behavior led to differences in the correlation between EMG amplitude and μ values in the proximal and distal regions.

Table 1

Median and interquartile range of the normalized centroid and % of segmented channels for all subjects during three consecutive intervals.

	Interval 1 (0–10% MVIC)	Interval 2 (10–20% MVIC)	Interval 3 (20–30% MVIC)
Centroid (%)	66 (64–69)	68 (65–75)	73 (66–86) *
Segmented Channels (%)	75 (45–88)	71 (54–98)	55 (32–98)

Abbreviation: MVIC = maximum voluntary isometric contraction.

* $p < 0.05$ to interval 1.

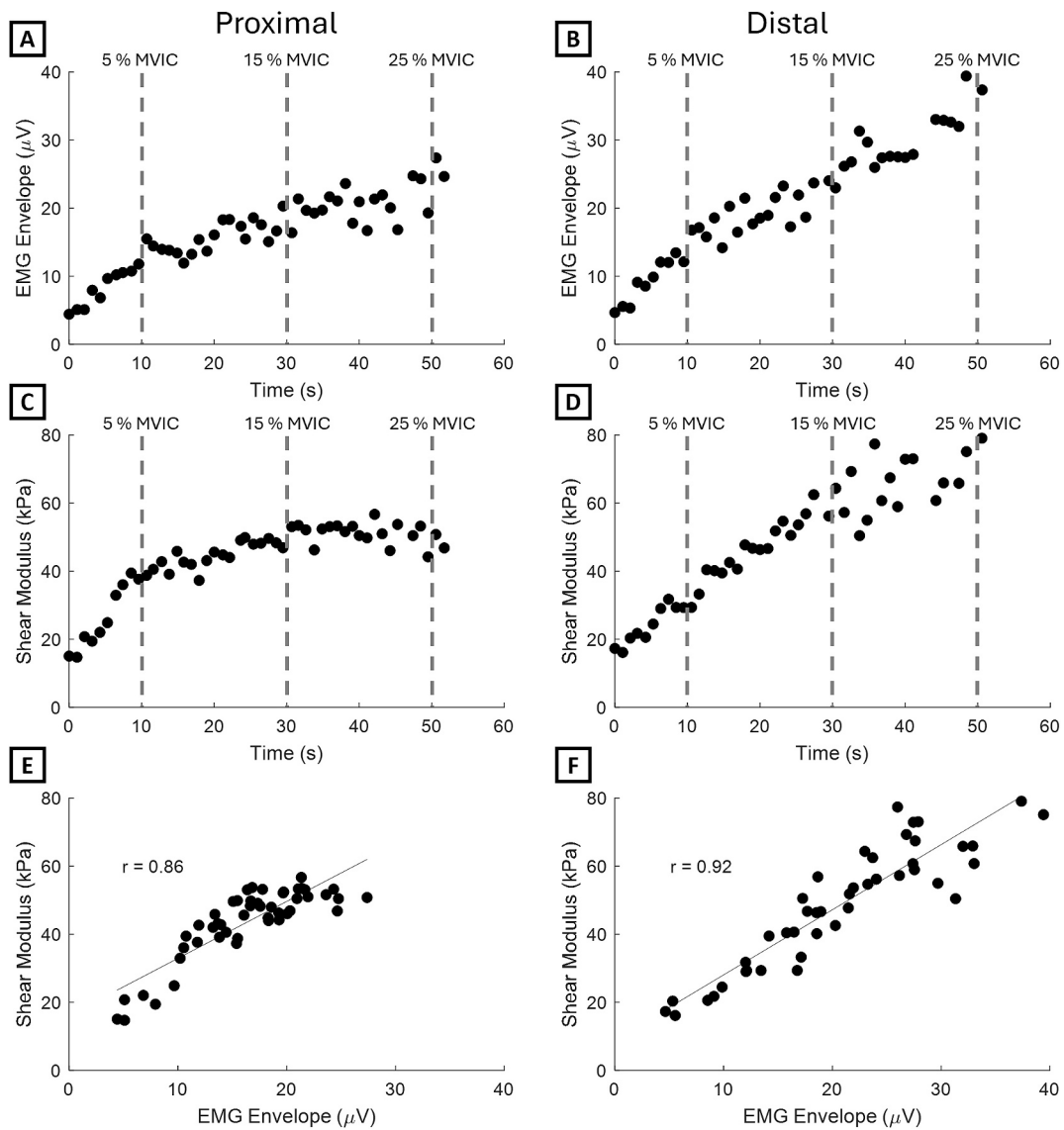


Fig. 3. Time trends of the EMG envelope for the proximal (A) and distal (B) portions of the MG, and time trends of μ for the proximal (C) and distal (D) portions. Correlation between EMG envelope amplitude and μ for the proximal (E) and distal (F) portions. All data refer to a single representative subject.

Although both muscle regions exhibited strong correlations, the distal region showed a higher correlation coefficient for the subject under analysis (Fig. 3E–F).

Group data confirm the significance of the relationship between EMG amplitude and shear modulus. Fig. 4A reports the boxplot of the

correlation coefficients between EMG envelopes and μ values for the 18 subjects tested. The two variables were strongly correlated for all subjects, in the two MG regions (mean \pm std: $r = 0.85 \pm 0.06$ proximally; $r = 0.91 \pm 0.05$ distally). In spite of the generally strong correlation, spatial differences in EMG-shear modulus relationship were observed.

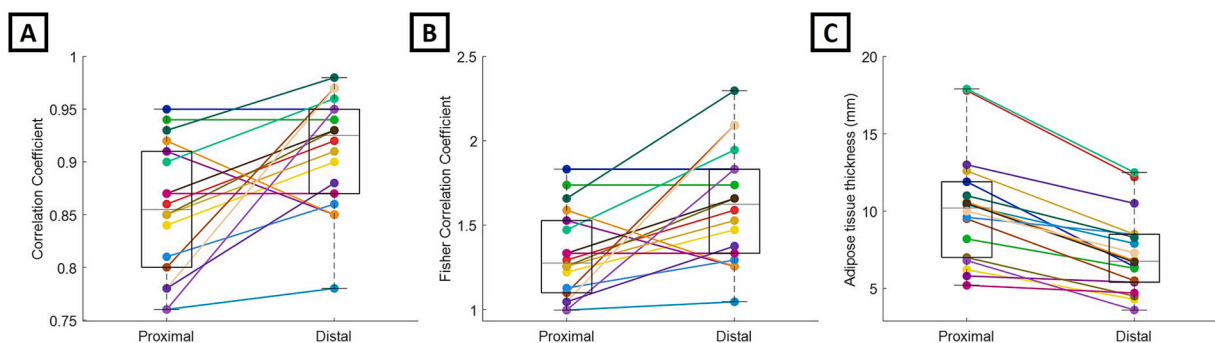


Fig. 4. (A) Boxplot of the correlation coefficients between EMG envelope amplitude and μ for all subjects. (B) Boxplot of the Fisher-transformed correlation coefficients. (C) Boxplot of the maximum adipose tissue thickness over the proximal and distal portions of the muscle.

The Fisher-transform correlation coefficient (Fig. 4B) was significantly lower ($p = 0.004$) for EMGs and images detected proximally ($r_f = 1.32 \pm 0.26$) than distally ($r_f = 1.63 \pm 0.34$). The 95% confidence interval (CI) for the mean difference in r_f was 0.11–0.50, and the effect size (Cohen's d) was 0.78, indicating a medium-to-large difference.

3.3. Subcutaneous differences between MG regions

The thickness of the adipose tissue above the proximal portion ($d_p = 10.2 \pm 3.6$ mm) was significantly greater than that above the distal portion ($d_d = 7.2 \pm 2.6$ mm; $p < 0.001$; Fig. 4C). Proximally, thickness values ranged from 5.2 mm to 17.9 mm, while distally, they ranged from 3.6 mm to 12.5 mm.

4. Discussion

From high-density EMGs and SSI data, the present study investigated whether, in the course of an isometric, low force-increasing contraction, excitation and stiffness increase similarly within MG. The results revealed a strong correlation between EMG envelope amplitude and μ across all subjects for both portions (Fig. 3E–F, Fig. 4A). However, the strength of this relationship was region-dependent, with a stronger association in the distal portion (Fig. 4B). These findings underscore the importance of considering muscle region-specificity when assessing EMG-stiffness relationships in the MG muscle.

4.1. Regional differences in MG excitation

The centroid of the segmented channels provides insight into the spatial distribution of MG excitation. A distal shift in the centroid between interval 1 and interval 3 suggests that more distal fibers were excited to a greater extent as force requirement increased. However, this interpretation must consider the influence of subcutaneous thickness on EMG amplitude. As reported in literature [36,37], subcutaneous tissue acts as a spatial filter, increasing the distance between electrode and source and thus reducing the amplitude of detected EMG signals. The observed proximo-distal differences in EMG amplitude could, therefore, be confounded by proximo-distal differences in subcutaneous tissue thickness. A normalization strategy has been adopted to mitigate this effect, by adjusting IED relative to subcutaneous thickness. Indeed, studies employing in-silico modeling [38] have demonstrated that increasing IED can partially compensate for the attenuation caused by thicker subcutaneous layers by capturing signals from a broader volume of muscle tissue. While subcutaneous thickness modulates absolute EMG amplitude, it does so consistently across force levels (i.e., intervals), ensuring the centroid was sensitive to regional changes in muscle excitation. Moreover, the IED considered for computing bipolar EMGs in the proximal and distal regions varied respectively from 10 to 20 mm and from 5 to 15 mm, with a presumably greater number of fibers being included in the detection volume of the proximal pair of electrodes (cf. Fig. 2A). Nevertheless, we acknowledge that residual spatial filtering effects cannot be fully excluded, and that the observed proximo-distal differences in EMG amplitude may still partially reflect methodological influences. More direct measures of regional neural drive, less dependent on EMG amplitude, would help to further support the interpretation of a stronger distal increase in excitation. Within this limitation, we therefore believe the proximo-distal differences in changes in EMG amplitude were predominantly due to regional changes in MG excitation rather than subcutaneous tissue filtering effects.

The considerable inter-subject variability observed in the percentage of segmented channels (Table 1) likely reflects a combination of physiological and methodological factors. From a physiological perspective, inter-individual differences in MG architecture (e.g. fascicle orientation, pennation angle) and individual motor unit recruitment strategies may influence the spatial distribution of excitation along the muscle [8].

From a methodological standpoint, variability in subcutaneous tissue thickness across subjects may affect EMG spatial selectivity and amplitude, thereby contributing to differences in the proportion of channels exceeding the segmentation threshold [36,37]. Importantly, despite this variability, the consistent distal shift of the excitation centroid with increasing force across subjects supports a robust physiological trend rather than a methodological artifact.

4.2. Gastrocnemius stiffness scales with excitation

Given previous evidence that fibers located in different regions of the MG may be activated independently [9,25], we examined the excitation–stiffness relationship separately in proximal and distal regions. The stronger coupling observed distally (Fig. 3 E-F; Fig. 4 A-B) may reflect higher local excitation levels (Fig. 3A-B; Table 1), resulting in an improved signal-to-noise ratio of the EMG and, consequently, a tighter association with shear modulus.

Our findings seem to confirm that excitation drives muscle stiffness, reinforcing previous evidence of a direct relationship between neural excitation and mechanical stiffness [18–20]. A key contribution of our work is the observation that the EMG- μ relationship varies across muscle regions. The underlying reason for this region-specific dependency needs to be discussed, since potential confounding factors should be considered when assessing the validity of SSI elastography measurements as, for example, ROI depth and muscle pennation angle. For instance, the SSI measurement depth has been shown to impact the μ value validity [39]. Although the subcutaneous tissue thickness was significantly greater in the proximal MG region than in the distal region (Fig. 4C), we adjusted the position of the shear wave mapping area to ensure the ROI remained within 3.5 cm of depth: within this limit μ measurements are reliable [39]. Regarding the regional variations in MG architecture, changes in pennation have been reported to change to a small extent (up to 1°) and similarly across the muscle during sub-maximal isometric plantar flexions up to 25% MVIC [40]. These considerations suggest the observed proximo-distal differences in EMG- μ relationship arise more likely from regional changes in MG excitation than SSI confounders.

It should be noted that we assessed the EMG- μ relationship during slow, force-increasing contractions, as imposed by technical limitation of our SSI machine. The sampling rate of SSI elastography (approximately 1 Hz) is dramatically lower than that of EMG (2000 Hz). Given our SSI system was specifically designed for clinical use, it does not support external input or output connections and therefore does not accept or issue any synchronization signals. Consequently, synchronization between SSI and HDsEMG recordings was performed manually, by initiating both acquisitions simultaneously. In virtue of the slow ramp protocol (0.5% MVIC per second), we believe any bias introduced by the manual synchronization to be negligible. Considering typical human reaction times (~ 200 – 250 ms [41]), the expected temporal offset between the two acquisitions is likely well below 1 s. Even a synchronization error on the order of one SSI frame (≈ 1 s) would correspond to a force mismatch of approximately 0.5% MVIC. Moreover, any residual bias would affect both proximal and distal measurements equally, thereby not confounding the comparison between regions. Extrapolation of current results to contractions imposing faster changes in force level may only proceed on the basis of sound judgement. If, however, the changes in neural excitation mainly explain the changes in muscle stiffness, it would seem plausible to expect that our results possibly extend to faster contractions.

4.3. Possible implications of regionalized EMG- μ relationship

For the first time, our results suggest that regional excitation pairs with regional stiffening, with local changes in muscle excitation being associated with local changes in muscle stiffening. More specifically, Figs. 2-4 indicate that excitation and the resulting tissue stiffening may

be confined locally within MG. If muscle mechanical properties during contraction are to be computed from SSI studies, this analysis should be paired with measurements of muscle excitation. More broadly, high-density EMG offers high spatial and spectral resolution for mapping muscle excitation across different regions of superficial muscles, while SSI provides insight into stiffness variations in both superficial and deep muscles—aspects that cannot be directly assessed through either technique alone. This issue is particularly relevant for large muscles, in which regional variations in excitation have been reported [42–44]. If controlling for excitation distribution during the task of interest (e.g., isometric ramp contractions, active stretching) is not viable, μ values may not reflect the whole muscle stiffness. Mechanistic and applied implications may stem as well from our study. For example, in addition to the spatial organization of fibers with different properties within the muscle [7,45], the regionalized EMG- μ relationship may contribute to optimizing fiber mechanical properties or other physiological factors such as blood flow determined by intramuscular pressure distribution [46]. While these issues remain to be explored, our study underscores the potential of combining high-density surface EMG and SSI for the study of muscle neuromechanical properties.

4.4. Limitations and future developments

The present findings should be interpreted in light of certain limitations. First, the experimental protocol was restricted to low-intensity force levels (up to 30% MVIC). While this choice was motivated by the technical constraints of SSI elastography and the need to ensure reliable shear wave propagation, the generalizability of the present findings to higher force levels remains to be established. In addition, the present investigation was limited to a single contraction modality, namely a controlled isometric force-increasing ramp. While this task was selected to ensure stable force output and to minimize non-stationarities that could compromise SSI measurements, muscle excitation and mechanical behavior during dynamic contractions may differ substantially. Therefore, the extent to which the present findings generalize to dynamic tasks remains to be established. Future studies should extend the combined HDsEMG–SSI approach to dynamic contractions to better capture task-dependent regional neuromechanical behavior. Another potential limitation of this study is its reliance on a young, healthy participant population, which restricts the direct generalizability of our findings to older individuals or those with musculoskeletal pathologies. This was a deliberate methodological choice, however, to minimize confounding variables such as muscle atrophy, sarcopenia, or changes in connective tissue that are often associated with aging or chronic conditions. By studying a homogeneous, healthy cohort, we were able to establish a clear baseline relationship between regional muscle excitation and stiffness without the influence of these extraneous factors. Finally, only the right leg was assessed, without screening for limb dominance or specific biomechanical factors such as flat foot. While these factors can influence muscle properties, we chose not to screen for them because our primary objective was to investigate the proximo-distal differences within the muscle. We assume that any such effects would influence both the proximal and distal regions similarly and therefore would not confound the regional differences that were the main focus of our study. Our methodology provides a robust framework for future research to specifically investigate the influence of these factors on regional neuromechanical properties in a targeted manner.

For future studies, combining EMG and SSI with additional modalities could provide a more comprehensive understanding of muscle neuromechanics. For example, the use of Doppler imaging available on some SSI systems could capture local changes in perfusion or muscle volume that may influence shear modulus independently of neural excitation [47]. Furthermore, ultrasound-based architectural measurements, including fascicle length and pennation angle, could help relate mechanical properties to structural and region-specific variations in muscle recruitment. Exploring these concurrent modalities could offer a

more comprehensive understanding of the determinants of muscle stiffness, improve interpretation of SSI–EMG relationships, and guide future studies aiming to link muscle architecture, excitation, and mechanics.

5. Conclusion

This study demonstrated that EMG excitation is strongly correlated with the μ measured by SSI elastography in proximal and distal portions of the MG during voluntary isometric contractions, with significantly higher correlation in the distal region of the muscle. The observed difference in correlation between the two regions may reflect regional variations in excitation along the muscle, with a tendency toward higher distal excitation. These findings reinforce the value of combining high-density EMG and SSI to characterize the neuromechanical properties of the MG, with potential advancements in their integration further enhancing the understanding of the mechanical and neurophysiological factors explaining the behavior of MG and other skeletal muscles, offering potential applications in clinical, rehabilitation, and sports science.

CRediT authorship contribution statement

Marco Daghero: Writing – original draft, Visualization, Software, Investigation, Formal analysis, Data curation, Conceptualization. **Maria Clara Albuquerque Brandão:** Writing – review & editing, Visualization, Software, Investigation, Formal analysis, Data curation. **Mara Terzini:** Supervision, Conceptualization. **Taian Martins Vieira:** Writing – review & editing, Visualization, Validation, Supervision. **Liliam Fernandes de Oliveira:** Writing – review & editing, Validation, Supervision, Project administration.

Declaration of competing interest

The authors declare that they have no known competing financial interests or personal relationships that could have appeared to influence the work reported in this paper.

Acknowledgements

This work was supported by the funding agencies FINEP (Grant no. 01.23.4567.89), FAPERJ, CAPES and CNPq. This publication is part of the project PNRR-NGEU which has received funding from the MUR – DM 351/2022.

Appendix A. Supplementary data

Supplementary data includes Table S1, reporting the distribution of subcutaneous adipose tissue thickness and electrode distances across the cohort for proximal and distal regions. Supplementary data to this article can be found online at <https://doi.org/10.1016/j.bspc.2026.110450>.

Data availability

Data will be made available on request.

References

- [1] T.M.M. Vieira, M.A. Minetto, E.F. Hodson-Tole, A. Botter, How much does the human medial gastrocnemius muscle contribute to ankle torques outside the sagittal plane? *Hum. Mov. Sci.* 32 (4) (2013) 753–767, <https://doi.org/10.1016/j.humov.2013.03.003>.
- [2] T.M.M. Vieira, U. Windhorst, R. Merletti, Is the stabilization of quiet upright stance in humans driven by synchronized modulations of the activity of medial and lateral gastrocnemius muscles? *J. Appl. Physiol.* 108 (1) (2010) 85–97, <https://doi.org/10.1152/jappphysiol.00070.2009>.

- [3] R.M. Howard, R. Conway, A.J. Harrison, Muscle activity in sprinting: a review, *Sport. Biomech.* 17 (1) (2018) 1–17, <https://doi.org/10.1080/14763141.2016.1252790>.
- [4] N.J. Cronin, J. Avela, T. Finni, J. Peltonen, Differences in contractile behaviour between the soleus and medial gastrocnemius muscles during human walking, *J. Exp. Biol.* 216 (5) (2013) 909–914, <https://doi.org/10.1242/jeb.078196>.
- [5] M.E. Héroux, C.J. Dakin, B.L. Luu, J.T. Inglis, J.S. Blouin, Absence of lateral gastrocnemius activity and differential motor unit behavior in soleus and medial gastrocnemius during standing balance, *J. Appl. Physiol.* 116 (2) (2014) 140–148, <https://doi.org/10.1152/jappphysiol.00906.2013>.
- [6] D.D. Shin, J.A. Hodgson, V.R. Edgerton, S. Sinha, In vivo intramuscular fascicle-aponeuroses dynamics of the human medial gastrocnemius during plantarflexion and dorsiflexion of the foot, *J. Appl. Physiol.* 107 (4) (2009) 1276–1284, <https://doi.org/10.1152/jappphysiol.91598.2008>.
- [7] T.M. Vieira, A. Botter, M.A. Minetto, E.F. Hodson-Tole, Spatial variation of compound muscle action potentials across human gastrocnemius medialis, *J. Neurophysiol.* 114 (3) (2015) 1617–1627, <https://doi.org/10.1152/jn.00221.2015>.
- [8] C. Avancini, L.F. De Oliveira, L.L. Menegaldo, T.M. Vieira, Variations in the spatial distribution of the amplitude of surface electromyograms are unlikely explained by changes in the length of medial gastrocnemius fibres with knee joint angle, *PLoS One* 10 (5) (2015) 1–16, <https://doi.org/10.1371/journal.pone.0126888>.
- [9] E.F. Hodson-Tole, I.D. Loram, T.M.M. Vieira, Myoelectric activity along human gastrocnemius medialis: different spatial distributions of postural and electrically elicited surface potentials, *J. Electromyogr. Kinesiol.* 23 (1) (2013) 43–50, <https://doi.org/10.1016/j.jelekin.2012.08.003>.
- [10] A. Haueise, G. Le Sant, A. Eisele-Metzger, A.V. Dieterich, Is musculoskeletal pain associated with increased muscle stiffness? evidence map and critical appraisal of muscle measurements using shear wave elastography, *Clin. Physiol. Funct. Imaging* 44 (3) (2024) 187–204, <https://doi.org/10.1111/cpf.12870>.
- [11] Z. Zhang, W. Wang, F. Li, and J. Guo, “Age and sex-related differences in elastic properties of the gastrocnemius muscle-tendon unit: an observational prospective study,” no. November, pp. 1–10, 2024, doi: 10.3389/fragi.2024.1455404.
- [12] G. Drost, D.F. Stegeman, B.G.M. van Engelen, M.J. Zwarts, Clinical applications of high-density surface EMG: a systematic review, *J. Electromyogr. Kinesiol.* 16 (6) (2006) 586–602, <https://doi.org/10.1016/j.jelekin.2006.09.005>.
- [13] R. Merletti, A. Holobar, D. Farina, Analysis of motor units with high-density surface electromyography, *J. Electromyogr. Kinesiol.* 18 (6) (2008) 879–890, <https://doi.org/10.1016/j.jelekin.2008.09.002>.
- [14] T.M. Vieira, A. Botter, The accurate assessment of muscle excitation requires the detection of multiple surface electromyograms, *Exerc. Sport Sci. Rev.* 49 (1) (2021) 23–34, <https://doi.org/10.1249/JES.0000000000000240>.
- [15] J. Bamber, et al., EFSUMB guidelines and recommendations on the clinical use of ultrasound elastography. part 1: basic principles and technology, *Ultraschall Med.* 34 (2) (Apr. 2013) 169–184, <https://doi.org/10.1055/s-0033-1335205>.
- [16] J.L. Gennisson, T. Deffieux, M. Fink, M. Tanter, Ultrasound elastography: Principles and techniques, *Diagn. Interv. Imaging* 94 (5) (2013) 487–495, <https://doi.org/10.1016/j.diii.2013.01.022>.
- [17] T. Shiina, JSUM ultrasound elastography practice guidelines: Basics and terminology, *J. Med. Ultrason.* 40 (4) (2013) 309–323, <https://doi.org/10.1007/s10396-013-0490-z>.
- [18] A. Nordez, F. Hug, Muscle shear elastic modulus measured using supersonic shear imaging is highly related to muscle activity level, *J. Appl. Physiol.* 108 (5) (2010) 1389–1394, <https://doi.org/10.1152/jappphysiol.01323.2009>.
- [19] R. Souron, et al., Sex differences in active tibialis anterior stiffness evaluated using supersonic shear imaging, *J. Biomech.* 49 (14) (2016) 3534–3537, <https://doi.org/10.1016/j.jbiomech.2016.08.008>.
- [20] Y. Yoshitake, Y. Takai, H. Kanehisa, M. Shinohara, Muscle shear modulus measured with ultrasound shear-wave elastography across a wide range of contraction intensity, *Muscle Nerve* 50 (1) (2014) 103–113, <https://doi.org/10.1002/mus.24104>.
- [21] L. Mesin, R. Merletti, T.M.M. Vieira, Insights gained into the interpretation of surface electromyograms from the gastrocnemius muscles: a simulation study, *J. Biomech.* 44 (6) (2011) 1096–1103, <https://doi.org/10.1016/j.jbiomech.2011.01.031>.
- [22] L. Vincent, et al., Quantifying active and passive stiffness in plantar flexor muscles following intermittent maximal isometric contractions using shear wave elastography, *Ultrasound Med. Biol.* 50 (12) (2024) 1987–1994, <https://doi.org/10.1016/j.ultrasmedbio.2024.09.004>.
- [23] K. Lima, N. Martins, W. Pereira, L. Oliveira, 67. Triceps surae elasticity modulus measured by shear wave elastography is not correlated to the plantar flexion torque. El módulo de elasticidad del tríceps sural medido por elastografía de ondas de corte no se correlaciona con el torque de flexión plantar, *Muscles. Ligaments Tendons J.* 7 (2) (2017) 347–352, <https://doi.org/10.11138/mltj/2017.7.2.347>.
- [24] R. Merletti, A. Rainoldi, and D. Farina, “Surface Electromyography for Noninvasive Characterization of Muscle,” *Exerc. Sport Sci. Rev.*, vol. 29, no. 1, 2001, [Online]. Available: https://journals.lww.com/acsm-essr/fulltext/2001/01000/surface_electromyography_for_noninvasive.5.aspx.
- [25] T.M.M. Vieira, I.D. Loram, S. Muceli, R. Merletti, D. Farina, Postural activation of the human medial gastrocnemius muscle: are the muscle units spatially localised? *J. Physiol.* 589 (2) (2011) 431–443, <https://doi.org/10.1113/jphysiol.2010.201806>.
- [26] T.M. Vieira, G.L. Cerone, A. Botter, K. Watanabe, A.D. Vigotsky, The sensitivity of bipolar electromyograms to muscle excitation scales with the inter-electrode distance, *IEEE Trans. Neural Syst. Rehabil. Eng.* 31 (2023) 4245–4255, <https://doi.org/10.1109/TNSRE.2023.3325132>.
- [27] P.A. Lynn, N.D. Bettles, A.D. Hughes, S.W. Johnson, Influence of electrode geometry on bipolar recordings of the surface electromyogram, *Med. Biol. Eng. Comput.* 16 (6) (1978) 651–660, <https://doi.org/10.1007/BF02442444>.
- [28] C. Toomey, K. McCreesh, S. Leahy, P. Jakeman, Technical considerations for accurate measurement of subcutaneous adipose tissue thickness using B-mode ultrasound, *Ultrasound* 19 (2) (2011) 91–96, <https://doi.org/10.1258/ult.2011.010057>.
- [29] T.M.M. Vieira, R. Merletti, L. Mesin, Automatic segmentation of surface EMG images: improving the estimation of neuromuscular activity, *J. Biomech.* 43 (11) (2010) 2149–2158, <https://doi.org/10.1016/j.jbiomech.2010.03.049>.
- [30] P. Bouchet, J.L. Gennisson, A. Podda, M. Alilet, M. Carrié, S. Aubry, Artifacts and technical restrictions in 2d shear wave elastography, *Ultraschall Der Medizin* 41 (3) (2020) 267–277, <https://doi.org/10.1055/a-0805-1099>.
- [31] D. MacDonald, A. Wan, M. McPhee, K. Tucker, F. Hug, Reliability of abdominal muscle stiffness measured using elastography during trunk rehabilitation exercises, *Ultrasound Med. Biol.* 42 (4) (2016) 1018–1025, <https://doi.org/10.1016/j.ultrasmedbio.2015.12.002>.
- [32] F. Cenni, M. Sukanen, A. Hernández-Belmonte, I. Laatikainen-Raussi, I. Vandekerckhove, and T. Finni, “The relationship between triceps surae muscle-tendon morphology and shear modulus across passive ankle range of motion in cerebral palsy,” *J. Biomech.*, vol. 192, no. September, 2025, doi: 10.1016/j.jbiomech.2025.112946.
- [33] R.M. Khair, M. Sukanen, T. Finni, Achilles tendon stiffness: influence of measurement methodology, *Ultrasound Med. Biol.* 50 (10) (2024) 1522–1529, <https://doi.org/10.1016/j.ultrasmedbio.2024.06.005>.
- [34] K. Kim, H.J. Hwang, S.G. Kim, J.H. Lee, W.K. Jeong, Can shoulder muscle activity be evaluated with ultrasound shear wave elastography? *Clin. Orthop. Relat. Res.* 476 (6) (2018) 1276–1283, <https://doi.org/10.1097/01.blo.0000533628.06091.0a>.
- [35] S. M. Barron, T. Ordóñez Díaz, F. Pozzi, T. Vasilopoulos, and J. A. Nichols, “Linear relationship between electromyography and shear wave elastography measurements persists in deep muscles of the upper extremity,” *J. Electromyogr. Kinesiol.*, vol. 63, no. September 2021, p. 102645, 2022, doi: 10.1016/j.jelekin.2022.102645.
- [36] T.A. Kuiken, M.M. Lowery, N.S. Stoykov, The effect of subcutaneous fat on myoelectric signal amplitude and cross-talk, *Prosthet. Orthot. Int.* (2003) 48–54, <https://doi.org/10.3109/03093640309167976>.
- [37] C. Nordander, et al., Influence of the subcutaneous fat layer, as measured by ultrasound, skinfold calipers and BMI, on the EMG amplitude, *Eur. J. Appl. Physiol.* 89 (6) (2003) 514–519, <https://doi.org/10.1007/s00421-003-0819-1>.
- [38] D. Farina, C. Cescon, R. Merletti, Influence of anatomical, physical, and detection-system parameters on surface EMG, *Biol. Cybern.* 86 (6) (2002) 445–456, <https://doi.org/10.1007/s00422-002-0309-2>.
- [39] A.M. Alfuraih, P. O’Connor, E. Hensor, A.L. Tan, P. Emery, R.J. Wakefield, The effect of unit, depth, and probe load on the reliability of muscle shear wave elastography: variables affecting reliability of SWE, *J. Clin. Ultrasound* 46 (2) (2018) 108–115, <https://doi.org/10.1002/jcu.22534>.
- [40] M.E. Héroux, P.W. Stubbs, R.D. Herbert, Behavior of human gastrocnemius muscle fascicles during ramped submaximal isometric contractions, *Physiol. Rep.* 4 (17) (2016) 1–10, <https://doi.org/10.14814/phy2.12947>.
- [41] D.L. Woods, J.M. Wyma, E.W. Yund, T.J. Herron, B. Reed, Factors influencing the latency of simple reaction time, *Front. Hum. Neurosci.* vol. 9, no. MAR (2015) 1–12, <https://doi.org/10.3389/fnhum.2015.00131>.
- [42] C. Sahinis, I.G. Amiridis, E. Kellis, Neuromechanical basis of region-specific differences and their implications for sport performance and injury prevention: a narrative review, *Eur. J. Appl. Physiol.* (2025), <https://doi.org/10.1007/s00421-025-05889-w>.
- [43] A. Samani, D. Srinivasan, S.E. Mathiassen, P. Madeleine, Variability in spatio-temporal pattern of trapezius activity and coordination of hand-arm muscles during a sustained repetitive dynamic task, *Exp. Brain Res.* 235 (2) (2017) 389–400, <https://doi.org/10.1007/s00221-016-4798-y>.
- [44] A. Fassbender, K. Karamanidis, and W. Potthast, “Regional differences in amplitude and spatial homogeneity of muscle activity in the biceps femoris long head,” *Eur. J. Appl. Physiol.*, no. 0123456789, 2025, doi: 10.1007/s00421-025-05783-5.
- [45] D. Kernell, “Muscle Regionalization,” *Can. J. Appl. Physiol.*, p. 22, 1998, doi: 10.1139/h98-001.
- [46] J.L. Van Leeuwen, C.W. Spoor, Modelling mechanically stable muscle architectures, *Philos. Trans. R. Soc. Lond. B Biol. Sci.* 336 (1277) (1992) 275–292, <https://doi.org/10.1098/rstb.1992.0061>.
- [47] Y. Kanaya, K. Konno, Y. Yamakoshi, N. Taniguchi, H. Watanabe, K. Takeshita, Evaluation of skeletal muscle elasticity using color Doppler shear wave imaging, *J. Ultrasound* 27 (1) (2024) 51–59, <https://doi.org/10.1007/s40477-023-00795-3>.